Developments in signal processing and interpretation in laser tapping

Perton, M.; Neron, C.; Blouin, A.; Monchalin, J.-P.

Publisher's version / Version de l'éditeur:
https://doi.org/10.1063/1.4789066
Review Of Progress In Quantitative Nondestructive Evaluation, 32, pp. 330-336, 2012-07-20

DEVELOPMENTS IN SIGNAL PROCESSING AND INTERPRETATION IN LASER TAPPING

M. Perton, C. Neron, A. Blouin, J.-P. Monchalin

National Research Council Canada, 75 de Mortagne Blvd, Boucherville, Québec, Canada, J4B 6Y4

ABSTRACT. A novel technique, called laser-tapping, based on the thermoelastic excitation by laser like laser-ultrasonics has been previously introduced for inspecting honeycomb and foam core structures. If the top skin is delaminated or detached from the substrate, the detached layer is driven into vibration. The interpretation of the vibrations in terms of Lamb wave resonances is first discussed for a flat bottom hole configuration and then used to determine appropriate signal processing for samples such as honeycomb structures.

Keywords: Laser-ultrasound, laser tapping, tapping, disbond, honeycomb structures.
PACS: 43.20.Ks, 43.35.Zc, 62.30.+d, 68.35.Np

INTRODUCTION

Laser-ultrasonics is by now a well known and mature nondestructive technique and successfully used for inspecting polymer matrix composites in aerospace [1]. Ultrasonic waves are first generated by a pulsed laser and then detected by a second laser coupled to an optical interferometer. The technique is particularly powerful for inspecting parts of complex shape. While the technique is very successful to find delaminations in laminates, difficulties are found for reliably detecting disbonds in material with natural voids such as honeycombs, foam core structures, or with large porosity and attenuation such as metallic foams. For this purpose, a novel technique called laser-tapping has been introduced [2, 3] and is here revisited. The principle of the technique is described next, and illustrated with examples of application to flat bottom holes and honeycomb structures. The interpretation of the induced vibrations in terms of Lamb wave resonances is first discussed for the flat bottom hole configuration and then used to determine appropriate signal processing for honeycomb structures.

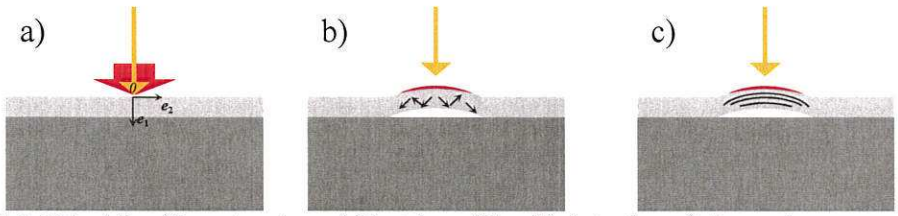

FIGURE 1. Principle of laser-tapping. a) Heat deposition, b) detection of ultrasonic waves and bending and c) detection of vibrations or low frequency oscillations.

PRINCIPLE OF LASER TAPPING AND EXPERIMENTAL SETUP

The principle of the laser tapping technique consists in depositing rapidly a localized quantity of heat by a laser pulse and in detecting the displacement generated at the same location during a few hundreds of microseconds. The technique can be seen as an equivalent to the conventional tap test used in industry. The purpose of the technique is to identify delaminations and unbounded areas by their "slow" surface motion (see Fig. 1).

The displacement of the surface results from two phenomena. First, the heat deposited on the top surface applies a local deformation mainly oriented along the surface, which causes a bulging of the surface (see Fig. 1-b). This bulging lasts all the time a temperature gradient exists and one can generally neglect heat diffusion during the time of the experiment. If the top layer is detached from its substrate, the bulging is larger and a part of the layer becomes no longer in contact with the substrate. Secondly, there is generation of ultrasonic waves (see Fig. 1-b). If there is a disbond, ultrasonics waves are trapped into the detached layer and reverberate back and forth through its thickness and between its edges. Finally, depending upon the geometry and mechanical properties, a standing wave pattern as vibration modes emerges (see Fig. 1-c).

The different phenomena are now discussed in the context of our experimental setup, i.e. according to the length and time scale of the experiment. The generation laser is a CO_2 TEA which delivers pulses of 120 ns duration at a wavelength of 10.6 μm with an energy varying from 50 mJ to 100 mJ. The beam is slightly focused to a spot of about 5 mm diameter. The excitation mechanism is purely thermoelastic and as such non-damaging. The surface displacement is detected by a single-frequency pulsed Nd:YAG laser which delivers pulses of 250 μs duration at a 1.064 μm wavelength. Its 20 mJ energy is only slightly less than the one of the generation laser but its absorption by the material is negligible. It is then not considered as a source of deformation. The generation and detection beams are also collinear. The scattered or reflected light of the detection beam is then collected and sent to a two-wave mixing photorefractive interferometer [4]. Since the vibrations are expected to have their frequencies in the range of 1 kHz to 1 MHz, the low frequency cut-off of the interferometer, which is determined by the pumping level applied to the crystal, is a compromise between, on one side, the interferometer sensitivity at low ultrasonic frequencies and, on the other side, its ability to adapt to ambient vibrations and the use of a pulsed detection laser.

Finally, laser-tapping and laser-ultrasonics are two techniques which bear some similarity, since they both use essentially the same hardware but they probe the material in distinct frequency ranges. Also, since the vibration mode corresponds to a coherent phase motion of the ultrasound waves, the displacement amplitudes generated by laser-tapping are quite large compared to those probe by laser-ultrasonics. Laser-ultrasonics and laser-tapping can be advantageously used concurrently in a combined inspection system that provides all the features of laser-ultrasonics, i.e. non contact, no surface preparation and ease of probing complex and large parts by rapid scanning.

APPLICATION TO FLAT BOTTOM HOLE

The laser tapping technique is first illustrated by considering the very simple defect of a flat bottom hole in a plate. The thickness of the membrane on top of the hole is denoted e and it radius is a (cf. Fig. 2). In the tested sample, a is equal to 6.223 mm and the ratio e/a is 0.3.

Figure 3-a shows the experimental signal. It corresponds to the normal displacement. A signal simulated using finite elements with LS-Dyna software is also shown in the same figure. Same geometrical and mechanical configurations of the experiment were used in the simulation. The experimental and simulated oscillations show almost the same behavior, but since the interferometer cuts the frequencies below 10 kHz, the static component of the displacement, denoted u_s in the simulated signal, is seen as a long decay. The bulging or bending component is then not correctly seen in the experiment.

A zoom of the first instants is also presented in the Fig. 3-b. The first tiny positive displacement at $t = 0$ µs is due to the thermal expansion of the layer illuminated in the direction normal to the surface, the so-called precursor in thermoelastic regime of laser-ultrasonic technique. It is then followed by a negative slope ($0 < t < 1$ µs) due, now, to the transverse (in-plane) expansion carried by skimming longitudinal waves. It implies a contraction in the normal direction (usually known as Poisson's effect). After, the negative slope, it is followed by a positive slope ($1 < t < 7$ µs) which leads a strongly oscillating displacement around the static value u_s. The strong oscillations are associated to the vibration of the membrane. Small oscillations at higher frequency are also visible on the top of the strong oscillation and are associated to the reverberation of the bulk waves through the thickness.

The characteristics of the strong oscillations are now studied in more details in the case when e is negligible comparing to a, i.e. when the membrane behaves as a thin rigidly clamped circular disc and when detection is performed at the center of the membrane. The lowest frequency of the vibration modes can be calculated according to membrane vibration theory by [5]:

$$\omega_1 = 0.47 \frac{e}{2\pi a^2} \sqrt{\frac{E}{\rho(1-\nu^2)}}, \tag{1}$$

where ρ is the mass density, E the Young's modulus and ν the Poisson's ratio of the isotropic material. The amplitudes of the resonances are proportional to [5]:

$$J_0(\gamma_m r) I_0(\gamma_m a) - J_0(\gamma_m a) I_0(\gamma_m r) \tag{2}$$

where J_0 and I_0 are the Bessel and modified Bessel function of first kind of order 0, r is the radius inside the membrane and γ_m is the m^{th} root of the equation:

$$J_0(\gamma_m a)/J_1(\gamma_m a) + I_0(\gamma_m a)/I_1(\gamma_m r) = 0 \tag{3}$$

No angular dependence is taken into account since it is a mode showing radial symmetry. The static bulging or bending is not taken into account in the equation (2) since it is negligible compared to e or a.

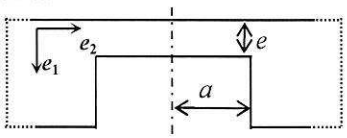

FIGURE 2. Flat bottom hole characteristics in a plate sample.

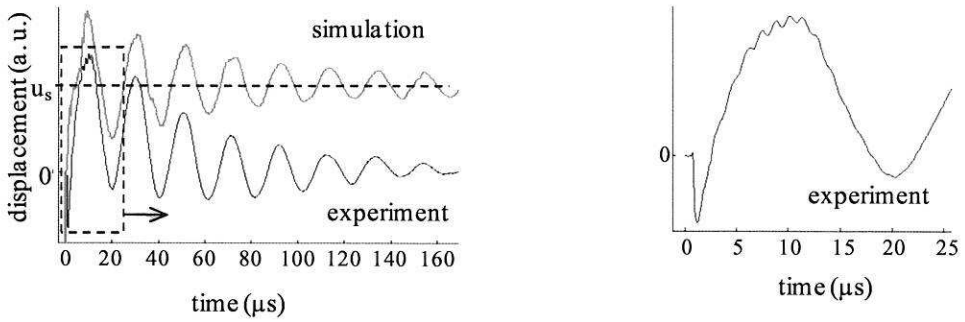

FIGURE 3. a) Experimental and simulated signals at the centre of a membrane such that e/a=0.3. b) Zoom at the beginning of the experimental signal showing higher frequency oscillations.

Another way to interpret these oscillations is to consider them as the displacement produced by Lamb waves. By considering that the A_0 anti-symmetric Lamb wave is dispersive, there are horizontal components k of the wave numbers for which the Lamb waves get into resonance inside the horizontal direction of the circular plate. These particular k verify then also the eq.(3), so that $k = \gamma_m$. The phase velocity associated with these wave numbers verifies the relation:

$$c_A = \omega/k \tag{4}$$

and its expression for a plate of thickness e is given by [6]:

$$c_A = \frac{ke}{2\sqrt{3}} c_P \text{ , with } c_P = \sqrt{\frac{E}{\rho(1-\nu^2)}}. \tag{5}$$

Here, c_P is the so-called plate velocity or velocity of the symmetric Lamb wave at low frequency. From (4) and (5) we deduce that the lowest frequency associated to the solution of (2) is:

$$\omega_{A0\_1} = \frac{\gamma_1^2 e}{2\sqrt{3}} c_P \text{ with } \gamma_1 a \approx 3.196 \text{ and for } e/a \ll 1 \tag{6}$$

which corresponds exactly to the solution (1).

The membrane vibration can then be interpreted as the resonance of a Lamb wave within the detached membrane. This interpretation of the vibrations in terms of Lamb wave resonances is of great interest for processing experimental signals, as it will be discussed in the next session.

INSPECTION OF A HONEYCOMB SAMPLE

Honeycomb structures allow reducing weight while keeping a high stiffness, and are then widely used in the aeronautic industry. Several defects, such as delaminations in the skin, detachments of the skin from the honeycomb ribs and crush cores likely to weaken the structure, as well as anomalies like excess of adhesive should be detected and identified. Figure 5-a shows a sketch of an honeycomb panel, prepared with the artificial defects previously mentioned. These defects are located within or close to its top surface. The panel consists of composite skins and aluminum ribs. The skins are about e = 1.1 mm thick and the ribs are about h = 12.7 mm high. The horizontal dimension of the sample is about 15 cm and the honeycomb unit cell diameter is 4.75 mm. The whole sample was scanned by the laser tapping technique. The step size of the scan was 1mm in both directions.

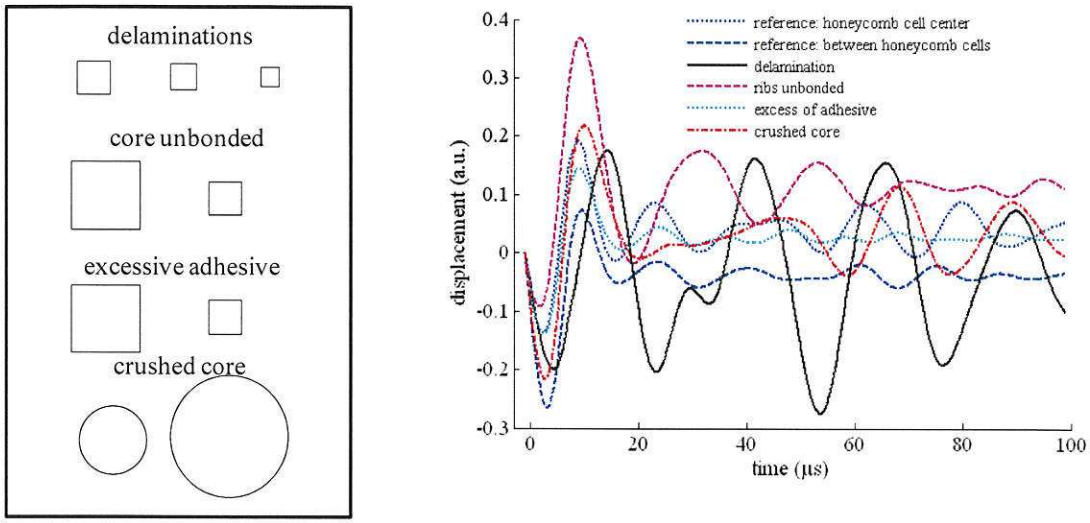

a) b)

FIGURE 4. a) Shape and localization of the artificial defects made in a honeycomb panel. b) Filtered signals for the several typical interrogating positions.

The signals obtained for typical positions are presented in Fig. 5-b. However, the low frequencies have been filtered out in order to reduce the sensitivity to the pulse temporal profile of the detection laser and to the amplitude of the static displacement. Experimental noise present at high frequencies (>200 kHz) is also filtered out by using time moving average.

The sound area shows some variability in the waveforms, which depend from the distance between the inspection position and the centre of the honeycomb cell. Two reference signals are then presented for illustration, one for which the inspection spot coincide with the cell center and another off-center. This variability makes data processing more difficult.

A first analysis often used consists in mapping the amplitude variation at a fixed time. But this analysis is rarely effective because of the variability in the sound area. It had been found successful only for defects close to the inspection surface (see Fig. 6a).

Another way for processing the data is in the frequency domain. The spectra of signals such as those shown in Fig. 5-b and recorded over a defect have frequencies peaks and amplitudes different from those recorded over a sound area. The defects are then revealed by mapping the frequency position of the peak of maximum amplitude (see Fig. 6b). However, such processing has several limitations. First, the shape of the defect being not always very regular, the resonance peaks are multiple and their amplitudes are consequently relatively low. Secondly, the oscillation can be rapidly attenuated and the peak frequency could become hardly visible, even if a large time window is taken. Also, when the defect has a large size, the oscillation period can be too long for the detection laser duration so only few cycles are visible, although one can detect the higher order modes occurring at higher frequencies which are excited when the laser beams enter the defect area [7].

A new method was consequently investigated. It corresponds to a compromise between the spectral and time analyses and consists in measuring the arrival time of one of the oscillation extrema (maximum or minimum) (see Fig. 6c). The analysis is made only over a limited time window centered on an extremum and its width is about the cell period. The choice of the extremum is discussed below. The process is then very sensitive to any transitory perturbation of the cell vibration period.

The results of the three processing methods are presented in Fig. 6a-b-c. All the artificial delaminations and ribs unbonded defects presented in Fig. 5-a can be identified

by all the processing methods. Additional unexpected anomalies are also revealed. Further work, using in particular through-transmission ultrasonics is planned to characterize these anomalies.

Since the presence of the honeycomb cells can represent a difficulty for defect identification, spatial averaging of several adjacent signals was performed. The result is presented for the whole sample in Fig. 7-a. Other very small unexpected anomalies are also revealed. It is also possible to perform the inspection from the side opposite to the defects. The results are shown in Fig. 7-b, which appears as it should be a mirror image of Figure 7a. The new analysis method was found very effective to reveal the defects from the opposite side. This is of major importance for practical use since both sides are not usually accessible for inspection.

The selection of the time windows analysis is now commented based on Lamb wave analysis. From the defect side, the identification of the defect is obtained by choosing a time window between 16 and 31 µs in order to analyze the first cycles of the honeycomb vibration. The process can be interpreted, in the presence of a defect with regular shape as an instantaneous measure of the vibration period. In that sense, it is quite similar to spectral analysis. But, in the presence of a defect with an irregular shape, the process is more similar to a measure of the arrival time of the A_0 Lamb waves reflected by the defect border. From the side opposite to the defects, identification of the defect is obtained by choosing a time window between 72 and 92 µs. The sensitivity to defects on the opposite side is due to the transmission of the out-of-plane motion of the A_0 Lamb waves through the ribs. The out-of-plane displacement in the skin implies an in-plane motion in the ribs which mainly propagates in turn as S_0 Lamb waves. The S_0 velocity at low frequency being very close to the longitudinal velocity, the minimal delay between the windows used to detect defects close to the inspected skin and the one opposite is calculated by the back and forth time of the longitudinal waves through the ribs of the core: $2hc_L \approx 4$ µs. However, since in case of a defect localized closed to the opposite skin, the vibrating detached part is composed of a skin patch stiffened by a number of ribs, a significantly longer time may be expected to have the mechanical energy distributed over its vibration modes. Consequently, higher sensitivity is then obtained by analyzing at a significantly later time.

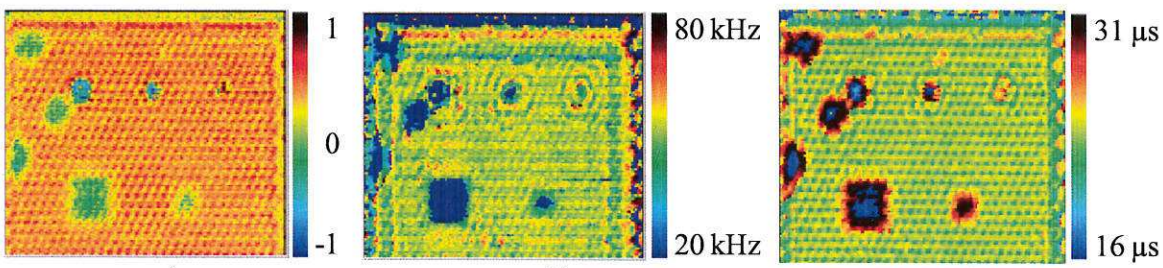

FIGURE 5. C-scan images obtained from the top surface and resulting from several data processes: a) normalized amplitude at about 12µs, b) frequency position of the maximum amplitude peak between [20, 80] kHz, c) time position of a minimum around [16, 31] µs.

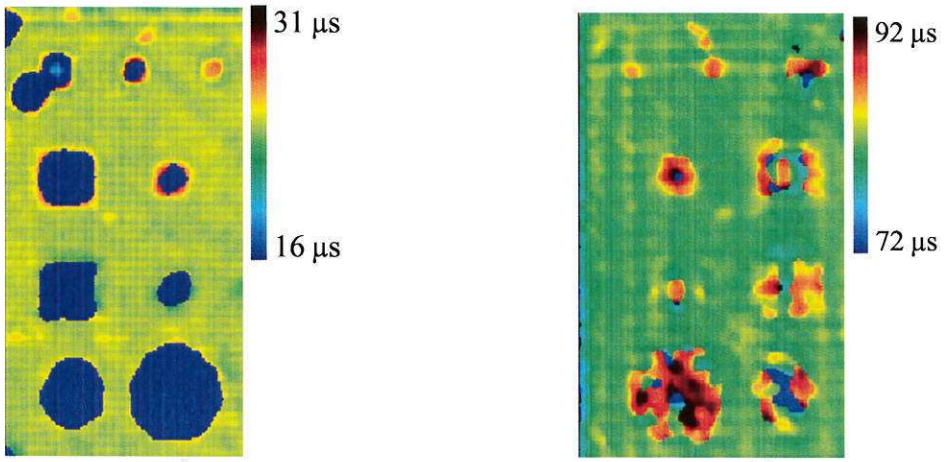

FIGURE 6. C-scan images of the whole sample obtained from the process as c) but with spatial traces averaging. The image a) (resp. b) is obtained from the surface inspection which is close (resp. opposite) to the defects, and corresponds to the time position of the extremum present between [16, 31] µs (resp. [72, 92] µs). .

CONCLUSION

We have reported a novel approach for processing laser tapping signals on honeycomb structures. This approach, first validated on membranes produced by flat bottom holes, is based on the interpretation of the observed signals as resulting from the propagation and resonance of Lamb waves within the defect area. Variability caused by the location of interrogation with respect to the honeycomb pattern have been significantly minimized by spatial averaging. Good results have been obtained for detecting all artificial defects on the test sample used, whether they are closed to the skin upon which generation and detection are performed or close to the opposite skin. Additional work is however required to characterize the unexpected anomalies found in the test panel.

REFERENCES

1. J-P Monchalin, Chapter 4, pp 79-115, in the book "Ultrasonic and Advanced Methods for Nondestructive Testing and Material Characterization", C H Chen Ed, World Scientific Publishing Co, 2007.
2. P. Cielo *et al.*, Materials Evaluation 43, pp. 1111-1116 (1985).
3. A. Blouin *et al.* "Detection of Skin Disbond in Honeycombs and Coating Detachment by a Laser Acoustic Technique", Review of Progress In QNDE vol 26, 2007
4. A. Blouin, J.-P. Monchalin, Appl. Phys. Lett. 65, pp. 932-934 (1994).
5. L. Kinsler, A. Frey, A. Coppens, J. Sanders "Fundamentals of Acoustics" Wiley, 2000
6. D. Royer and E. Dieulesaint, "Elastic Waves in Solids", Masson, Paris, 1996.
7. J.-P. Monchalin, A. Blouin, B. Campagne, *Method of Assessing Bond Integrity in Bonded structures*, US patent #8,004,689.